A High-Performance Sensorless DTC Strategy Based on MRAS for Induction Motors: Experimental Validation

Houssam Ech-chaouy[1*], *Aziz* Derouich[1], and *Said* Mahfoud[1, 2]

[1]Industrial Technologies and Services Laboratory, Higher School of Technology, Sidi Mohamed Ben Abdellah University, Fez 30000, Morocco.
[2]Polydisciplinary laboratory of sciences, technologies, and societies, Sultan Moulay Slimane University, Khenifra, Morocco.

Abstract. Direct Torque Control (DTC) is one of the most widely adopted techniques in industrial applications due to its numerous advantages. While it effectively reduces torque ripple, its performance is further enhanced through the use of hysteresis-based models, PID speed controllers, and switching tables that generate variable frequencies. However, the operation of induction motors at low speeds—particularly the variations in stator resistance—significantly affects their performance. To address these challenges and optimize motor behavior, this study proposes an improved control approach. The control strategy has been enhanced through a sensorless method based on the Model Reference Adaptive System (MRAS) algorithm. This allows real-time estimation of speed, torque, and flux, eliminating the need for costly physical sensors. The MRAS algorithm not only reduces system complexity and cost but also adapts dynamically to changes in load and voltage, thereby improving overall reliability and energy efficiency. Moreover, it helps minimize component wear, thus extending the operational lifespan of the motor.
The proposed MRAS-based sensorless DTC technique has been simulated using MATLAB/Simulink and implemented using DSpace DS1104, demonstrating significant improvements in motor performance and control system behavior.

Keywords: Sensorless speed, Model Reference Adaptive System, induction motor, Direct Torque Control.

1 Introduction

The induction machine (IM) is highly valued in the industrial sector for its advantages, including simple construction, reliability in electromechanical energy conversion, robustness, affordability, and low maintenance requirements [1]. However, its multivariable model is nonlinear and strongly coupled due to time-varying parameters.

* Corresponding author: houssam.echchaouy@usmba.ac.ma

Additionally, some variables are inaccessible for measurement, necessitating the use of state observers, which can reduce the robustness of machine control [2].

Despite these challenges, the presence of induction motors in variable-speed drives has grown significantly over the years. They are now widely used in various applications such as electric vehicles, elevators, pumping systems, ventilation, and many others [3, 4]. This growth has been facilitated by the evolution of static power converters and management systems, as well as the emergence of faster computing techniques, such as digital signal processing (DSP), which have helped reduce operating costs.

The implementation of complex control algorithms is now more feasible, and many electrical applications require their use. For applications involving electric motors, it is essential to employ variable-speed drives associated with appropriate control systems to ensure a wide operating range and excellent dynamic performance. Most applications frequently utilize vector control and direct torque control methods [5, 6].

Blaschke [5] introduced field-oriented control (FOC) to achieve a similar decoupling between magnetic flux and the electromagnetic aspects of a separately excited DC machine. This method enables high-level dynamic performance. However, practical implementation has revealed that FOC is extremely sensitive to parametric fluctuations [7], particularly changes in rotor resistance, which is closely associated with the angle of the flux direction. To address the specific disadvantages observed with FOC in induction machines, Takahashi [6] developed direct torque control (DTC).

Direct torque control (DTC) first appeared in the 1980s as a straightforward control method for induction motors. The work of Takahashi and Ohmori (Takahashi and Ohmori, 1989) formed the basis for a control algorithm that is capable of tracking stator and rotor flux within hysteresis bands. While modulation methods, such as pulse-width modulation (PWM), and scalar control methods, such as coordinate transformation techniques (known as DTC), use PWM or (like the path the torque approaches) and scalar control (like hysteresis bands), when properly constructed and executed, DTC provides a relatively direct decoupling of the management of flux and torque.

The principle of DTC, like all motor control strategies, is to command actions applied to switches within (e.g., Induction motors, double-fed cage induction motors). For the example illustrated in DTC, this command is applied to the inverter switches feeding an induction machine (specifically a 3-phase squirrel-cage machine). And intentionally maintains a natural decoupling between flux and torque.

The performance of the DTC approach provides many advantages, such as dynamics, robustness, parameter insensitivity, ease of implementation, and compelling performance, but is limited somewhat by the hysteresis comparator. The hysteresis comparator allows for variable frequency operation, but it is impractical at best; it is typically not a standard comparator application. However, finite frequency sampling can lead to a pseudo-random overshoot of the hysteresis band, which may affect low-speed operation, particularly due to variations in motor resistance. Moreover, the application of classic DTC to asynchronous machines can induce torque oscillations that are disruptive for users. These oscillations can excite mechanical resonances, causing vibrations and audible noise, which contribute to the premature aging of the machine (Mahfoud et al., 2021a).

In recent years, multiple researchers have put forth proposals to improve the operation of conventional torque control techniques using artificial intelligence-based techniques such as neural networks, fuzzy logic, and hybrid control strategies. When utilizing these techniques, there is no required expertise in a particular mathematical model. These techniques demonstrate good robustness to parametric variation.

These techniques have shown significant success in the identification and control of nonlinear systems. In DTC, they allow the control of switching frequency and provide a quickly responding flux and torque with reduced distortion. Although these strategies are proposed, they also have the following disadvantages: DTC is more complicated in its internal structure and uses a complicated computer. Therefore, it is essential to eliminate physical sensors and apply estimation methods to enhance control robustness and reduce costs [8, 9]. This

approach involves replacing the physical sensor with algorithms, such as estimators or observers, where the speed and position of the rotor are inferred from the electrical parameters of the machine rather than measured directly.
The literature presents various methods for sensorless speed control of induction machines. Among these methods are the Luenberger adaptive observer (LO), the extended Kalman filter (EKF), and the model reference adaptive system [10-14].
The EKF is one of the earliest observers to achieve significant success due to its ease of implementation, even for complex nonlinear systems [10]. Its primary objective is to analytically approximate the system states using stochastic methods to converge to an operating point. However, a notable drawback is the lack of a comprehensive demonstration of its convergence [11].
Another approach is the direct calculation method (DCM), which relies on the machine model to facilitate speed estimation based on rotor flux values. Despite its superior performance, simplicity, and reduced computational time, this method is limited by its dependence on rotor parameters, which undermines overall control effectiveness [12].
The Luenberger observer (LO) [13] allows for the estimation of unmeasurable states through error correction based on observed states. However, as previously noted, these techniques generally exhibit poor performance at low speeds and are sensitive to parameter variations.
Methods based on the Model Reference Adaptive System (MRAS) technique remain relevant due to their ease of application and low computational demand [14].
The MRAS method employs an adaptive system that utilizes two distinct flux models: a reference model that does not include speed and an adjustable model that depends on speed. The adaptability algorithm, which produces an estimated speed, is driven by the error resulting from the divergence between the two models. However, it has a significant drawback: its performance deteriorates at low speeds and is sensitive to variations in rotor resistance, particularly when using a traditional PID controller.
This approach does not perform very well when the system experiences large disturbances, and its gain values vary with the motor parameters, which are not constant [15].
In this paper, we propose a new concept: the DTC sensorless scheme with an MRAS estimator. The goal will be to replace the PI controller, 3 hysteresis comparators, and switching tables with neural network-based controllers. This mixed approach seeks to overcome sensitivity to parametric fluctuations as a result of the PI controller and the generation of variable logic signals, leading to harmonic increases in transmitted signals.
Ultimately, this method aims to achieve the following objectives:

- Adaptation of DTC control to the parametric variations of the machine.
- Improvement of speed performance (response time, settling time, overshoot).
- Reduction of flux and torque ripple.

The presentation of the paper is organized as follows: Sections 1 and 2 provide information on the inverter model and the induction motor development. In Section 3, we investigate Direct Torque Control (DTC) analytically, and we discuss the design and development of a Model Reference Adaptive System (MRAS) estimator in Section 4, which is suitable for the implementation of the control strategy. Sections 5 and 6 give the details of implementing the proposed method in MATLAB/Simulink, and subsequently its physical implementation on the dSPACE 1104 board, and the resultant analysis of the simulation and experimental results. We conclude with a summary of the outcomes and the recommended future directions.

2 Mathematical model of the induction motor

The correct mathematical model for examining the DTC in an IM is the two-phase model in (α, β) coordinates, which is governed by equations [16].

Electrical equations:

$$\begin{cases} v_{s\alpha} = R_s.i_{s\alpha} + \dfrac{d\psi_{s\alpha}}{dt} \\ v_{s\beta} = R_s.i_{s\beta} + \dfrac{d\psi_{s\beta}}{dt} \\ v_{r\alpha} = 0 = R_r.i_{r\alpha} + \dfrac{d\psi_{r\alpha}}{dt} + \omega_m.\psi_{r\beta} \\ v_{r\beta} = 0 = R_r.i_{r\beta} + \dfrac{d\psi_{r\beta}}{dt} - \omega_m.\psi_{r\alpha} \end{cases} \quad \textbf{(1)}$$

Magnetic equations:

$$\begin{cases} \psi_{s\alpha} = L_s i_{s\alpha} + L_m.i_{r\alpha} \\ \psi_{s\beta} = L_s i_{s\beta} + L_m.i_{r\beta} \\ \psi_{r\alpha} = L_r i_{r\alpha} + L_m.i_{s\alpha} \\ \psi_{r\beta} = L_r i_{r\beta} + L_m.i_{s\beta} \end{cases} \quad \textbf{(2)}$$

Mechanical equations:

$$\begin{cases} T_{em} = p.(\psi_{s\alpha} i_{s\beta} - \psi_{s\beta} i_{s\alpha}) \\ J.\dfrac{d\Omega}{dt} + f.\Omega = T_{em} - T_r \end{cases} \quad \textbf{(3)}$$

The voltage source inverter (2L-VSI) model can be viewed as a system of six switches, which are assumed to be controlled by analytic values [17]. The configuration of the 2L-VSI is depicted in Figure 1. Each of the six idealized electronic switches may represent transistors (IGBTs) with diodes. The voltage vectors are expressed in the stationary reference frame (α, β) [18].

Table 1. Voltage source inverter table.

$\mathbf{V_i}$	**S = (Sb Sa Sc)**	$\mathbf{V=V_\alpha + V_\beta}$
V_0	(000)	0
V_1	(100)	(2/3).Vdc
V_2	(110)	(1/3).Vdc + j (√3/3).Vdc
V_3	(010)	-(1/3).Vdc + j (√3/3).Vdc
V_4	(011)	- (2/3).Vdc
V_5	(001)	-(1/3).Vdc- j (√3/3).Vdc
V_6	(101)	(1/3). Vdc- j (√3/3).Vdc
V_7	(111)	0

Figure 1 shows the voltage vectors that the 2L-VSI delivers.

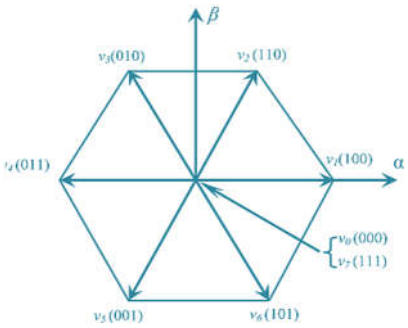

Fig. 1. Voltage vectors delivered by 2L-VSI.

3 Direct torque control

DTC is an advanced algorithm that implements control sequences for a voltage source inverter to obtain direct regulation of motor torque and flux. DTC utilizes hysteresis regulators to regulate the amplitudes of flux and electromagnetic torque such that they both remain within predetermined error bands. The outputs of the hysteresis regulators and the position of flux are used to determine which voltage vectors should be selected. The inverter can generate seven phase planes; therefore, it will have eight output voltage sequences.

3.1 Principle of the DTC strategy

Command control of the electromagnetic torque and the stator flux [1]. The output of the hysteresis controllers enables the 2L-VSI to choose switching states from a switching table. The DTC strategy is based on the rotor speed being assumed very high, so the stator resistance voltage drop is negligible in the stator voltage equation [19, 21]. Then, because this voltage drop is neglected in this part of the equation, the voltage vector to the inverter can vary the stator flux quite effectively. An overall model of DTC is summarized in Figure 2. At each sample period, Ts, static measurements of the electromagnetic torque and the flux are taken. The only information needed to estimate the electromagnetic torque and the flux is the knowledge of the voltage vector applied and instantaneous measurements of the stator currents.
Static measurements are only done with knowledge of the applied voltage vector. The DTC is beneficial for a torque schematic because the DTC is fairly insensitive to the parametric variation of the motor and has a fast and accurate torque response. The scheme is intended for direct torque and flux control of the machine. The operation of the motor is governed by a value that is averaged with a computed and static holding (desired) value. The portion of the value determines, based on a computed voltage, which voltage is appropriate to apply. The process, as illustrated in Fig. 1, uses a comparator and a lookup to apply the appropriate voltage.

3.2 Vectors control of stator flux

The formulas below show how to find the stator's magnetic fluxes in the reference frame (α, β). The mapping of magnitudes and positions of these fluxes is defined by the relationship below (Mahfoud et al., 2022a).

$$\bar{\psi}_s(t) = \int_0^t (\bar{V}_s + R_s.\bar{I}_s).dt \quad \& \quad \begin{cases} \hat{\psi}_s = \sqrt{\hat{\psi}_{s\alpha}^2 + \hat{\psi}_{s\beta}^2} \\ \theta_s = arctg\left(\dfrac{\hat{\psi}_{s\beta}}{\hat{\psi}_{s\alpha}}\right) \end{cases} \tag{4}$$

Using a mathematical formula from the (α, β) reference frame, one can compute an electromagnetic torque.

$$\hat{T}_{em} = p.(\hat{\psi}_{s\alpha}.i_{s\beta} - \hat{\psi}_{s\beta}.i_{s\alpha}) \quad \textbf{(5)}$$

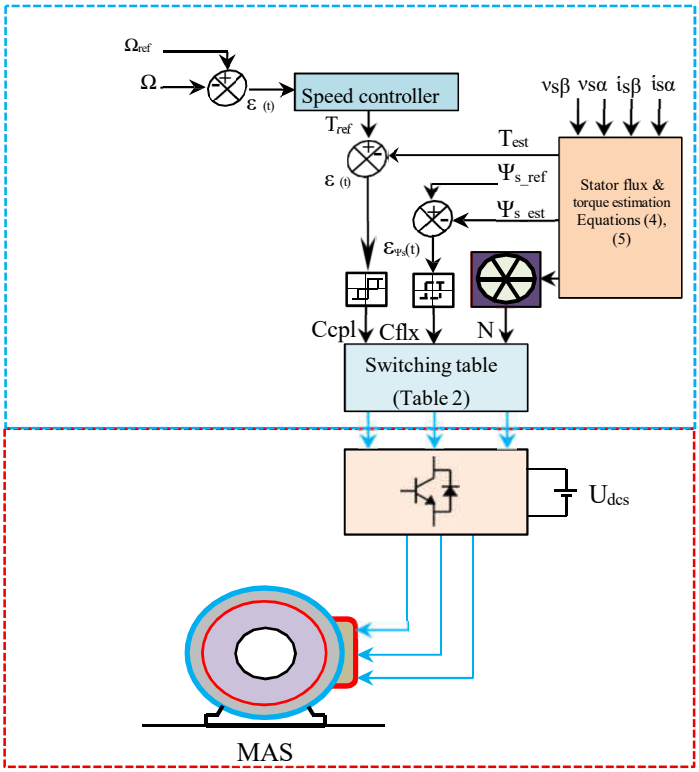

Fig. 2. Proposed Structure of Classic DTC.

3.3 Hysteresis comparators

The system utilizes two two-level hysteresis comparators to constrain the end of each flow vector in the circular band depicted in Figure 3. Additionally, Figure 4(a) illustrates a three-level hysteresis comparator, which generates an electromagnetic torque (in the clockwise and counterclockwise directions) generated by the motor. The comparators produce either positive or negative torque.

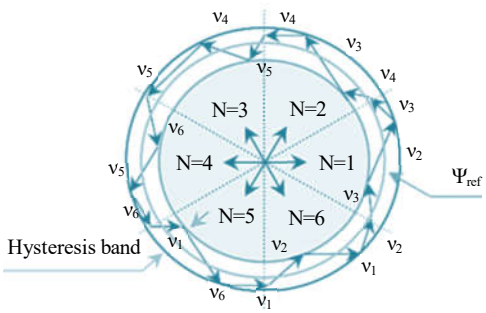

Fig. 3. Magnetic flux trajectory.

Fig. 4. Hysteresis comparators (a) of the three-level torque (b) of the two-level flux.

3.4 Switching table construction

The decision on which voltage vector will be applied should consider the sector in addition to the rotations of torque and flux. A truth table that identifies the voltage vector based on the sector (to indicate where the motor is) is shown in Table 2.

Table 2. Inverter sequences.

	Sector						
Ψ	**Ccpl**	**S_1**	**S_2**	**S_3**	**S_4**	**S_5**	**S_6**
1	1	v_2	v_3	v_4	v_5	v_6	v_1
	0	v_7	v_0	v_7	v_0	v_7	v_0
	-1	v_6	v_1	v_2	v_3	v_4	v_5
0	1	v_3	v_4	v_5	v_6	v_1	v_2
	0	v_0	v_7	v_0	v_7	v_0	v_7
	-1	v_5	v_6	v_1	v_2	v_3	v_4

4 Model reference adaptive system estimator

For most industrial applications, closed-loop feedback data is required. With the mechanical speed sensors, there was much less information available. The use of mechanical speed sensors results in more costs, congestion, low reliability, sensitivity to mechanical noise, and an inability to adapt to hostile environments. For these reasons, many of the research methods have focused on sensorless electrical drives to eliminate mechanical tools. Because of its relative simplicity and speed of computation, the MRAS principle (sliding mode) speed estimation methods have gained some notoriety [22].

The estimator modifies its structure by the error; that is, the discriminator between the reference model and the adjustable model is the error.

About Figure 5, the MRAS algorithm utilizes the stator flux vector components (ψ_{as}, $\psi_{\beta s}$) as a reference using the available voltage (v_{as}, $v_{\beta s}$) and current (i_{as}, $i_{\beta s}$) measurements.

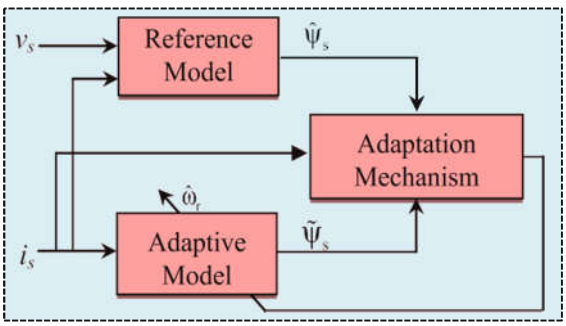

Fig. 5. Model Reference Adaptive System estimator.

4.1 Reference Model

The reference model in the (α, β) frame, derived from the mathematical design of the electrical machine, is given by the stator flux vector components (ψαs, ψβs) and expressed in terms of the available stator quantities:

$$\begin{cases} \hat{\varphi}_{\alpha s} = \int (V_{\alpha s} - R_s \times I_{\alpha s}) \\ \hat{\varphi}_{\beta s} = \int (V_{\beta s} - R_s \times I_{\beta s}) \end{cases} \quad \textbf{(6)}$$

4.2 Adjustable model

The equations of the adjustable model can be written as follows:

$$\begin{cases} \tilde{\varphi}_{\alpha s} = \dfrac{L_r}{R_r + L_{rs}} (\sigma \times L_s \times \hat{\omega}_r \times i_{\beta s} + \dfrac{L_s}{L_r} (R_r + \sigma L_{rs}) \times i_{\alpha s} - \hat{\omega}_r \times \hat{\varphi}_{\beta s} \\ \tilde{\varphi}_{\beta s} = \dfrac{L_r}{R_r + L_{rs}} (-\sigma \times L_s \times \hat{\omega}_r \times i_{\alpha s} + \dfrac{L_s}{L_r} (R_r + \sigma L_{rs}) \times i_{\beta s} + \hat{\omega}_r \times \hat{\varphi}_{\alpha s} \end{cases} \quad \textbf{(7)}$$

4.3 Adaptation mechanism

An adjustment device, which is dependent on the difference between the reference state and the adjustable state, generates the estimated speed. The adjustment mechanism affects the system stability while ensuring that the estimated value converges. Both Ki and Kp are positive gain values. The expected speed is represented by wr when substituting into (8).

$$\hat{\omega}_r = F(K_p) + F(K_i) \quad \textbf{(8)}$$

Where:

$$\begin{cases} F(K_p) = K_p (\lambda_{\alpha s} i_{\beta s} - \lambda_{\beta s} i_{\alpha s}) \sigma L_s \\ F(K_i) = K_i \int_0^{\tau} (\lambda_{\alpha s} i_{\beta s} - \lambda_{\beta s} i_{\alpha s}) \sigma L_s) d\tau \\ \lambda_{\alpha s} = \hat{\varphi}_{\alpha s} - \tilde{\varphi}_{\alpha s} \\ \lambda_{\beta s} = \hat{\varphi}_{\beta s} - \tilde{\varphi}_{\beta s} \end{cases} \quad \textbf{(9)}$$

The following figure shows a synoptic diagram of the DTC control optimized with the MRAS algorithm.

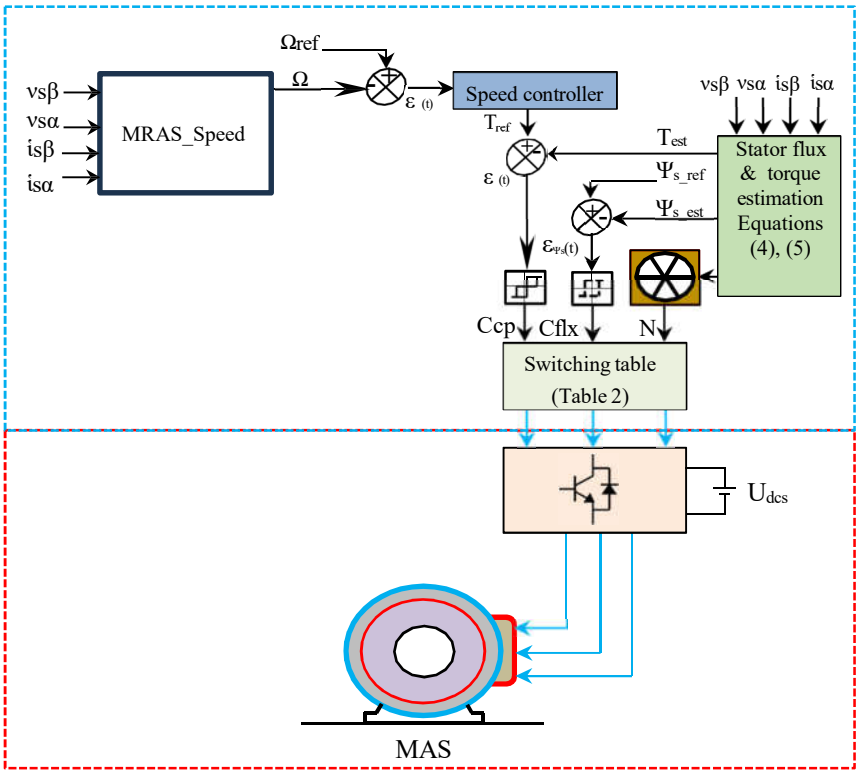

Fig. 6. Proposed Structure of DTC-MRAS.

5 Results and interpretation

This study, conducted in this paper, investigates direct torque control for the squirrel-cage asynchronous machine. This DTC has been improved through a real-time acquisition of the rotational speed of the rotor using the MRAS algorithm.

The following figures (7, 8, 9, 10, and 11) illustrate the evolution of current, speed, torque, and magnetic flux for the DTC_MRAS control compared to the DTC control. The machine operates at variable speeds and torques ranging from -157 rad/s to 157 rad/s and from -10 Nm to 10 Nm. We divide the results into two parts: simulation using MATLAB/Simulink and practical validation in the specific environment of dSPACE 1104.

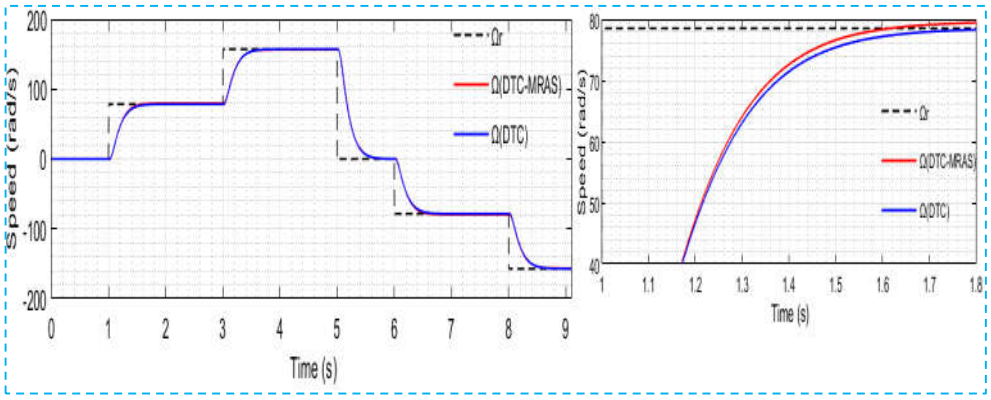

Fig. 7. Speed variation responses of the DTC and DTC_MRAS.

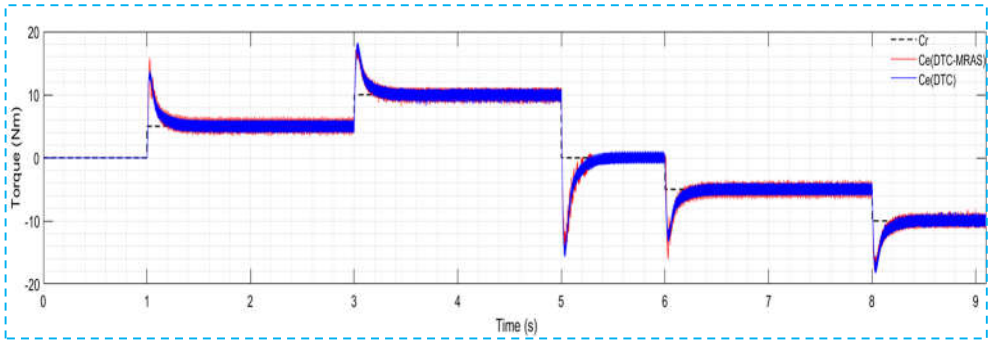

Fig. 8. Torque curves of the DTC controller and DTC-MRAS.

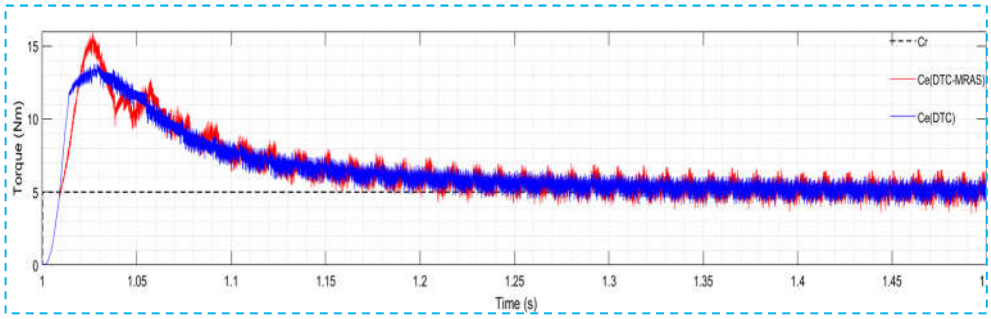

Fig. 9. Zoom of torque curves for the DTC controller and DTC-MRAS.

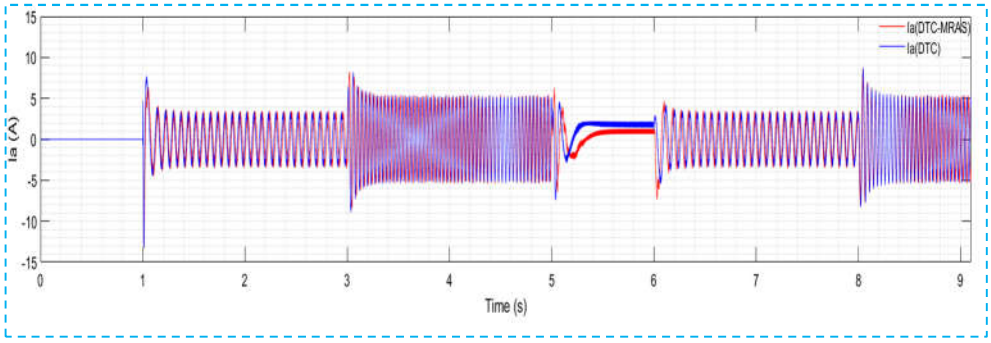

Fig. 10. Waveforms of the stator currents for the DTC and DTC-MRAS control.

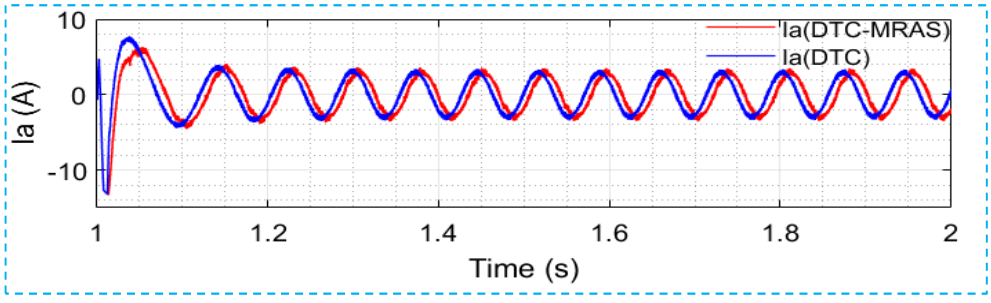

Fig. 11. Zoom of the waveforms of the stator currents for the DTC and DTC-MRAS control, along with a close-up of the currents.

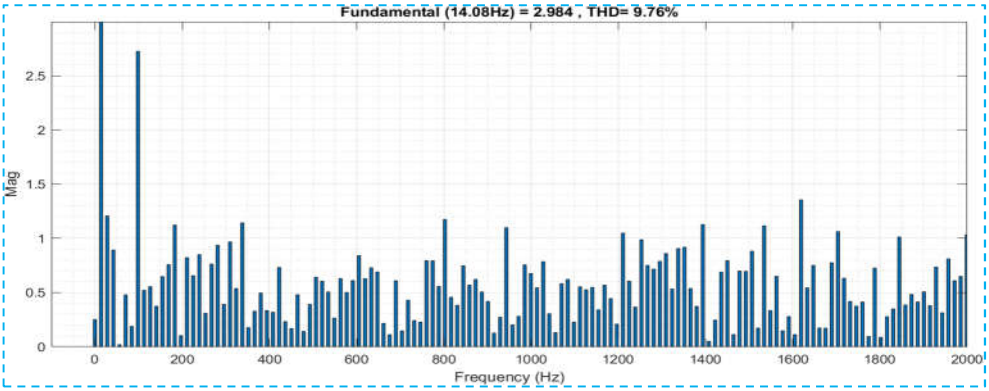

Fig. 12. THD in the stator current (Isa) of the DTC.

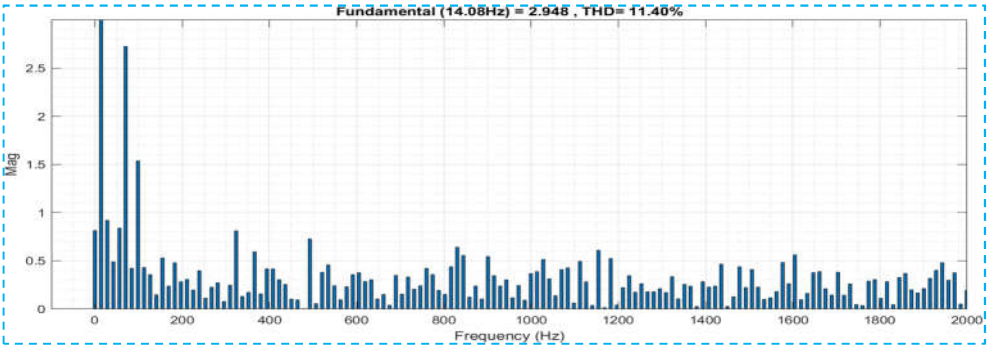

Fig. 13. THD in the stator current (Isa) of the DTC-MRAS.

The presented figures illustrate the variation and evolution of the machine's characteristic quantities, such as the stator electric current and stator magnetic flux, as well as mechanical quantities like rotor speed and mechanical torque. This section presents the results obtained for DTC control, as well as for DTC control using the MRAS algorithm. Additionally, this part includes a comparative study between the two methods.

It can be observed from the figures that the speed accurately tracks the variable reference between -157 rad/s and 157 rad/s, and that the machine can start under a variable load (between -10 Nm and 10 Nm) with both DTC and DTC-MRAS control.

Figure 7 shows the evolution of the mechanical speed for the two approaches, wr (DTC) and wr (DTC-MRAS). It can be seen that the MRAS-based control exhibits a slightly higher speed compared to the control without MRAS.

Figure 8 shows the evolution of the mechanical torque for the two approaches, DTC and DTC-MRAS. It is noted that the MRAS-based control exhibits additional fluctuations compared to the control without MRAS.

Figure 10 shows the evolution of the stator electric current for the two approaches, Ias (DTC) and Ias (DTC-MRAS). It is observed that the MRAS-based control introduces a phase shift compared to the control without MRAS. This difference may be attributed to the sampling frequency. It is significant and calls for improvements. The performance of MRAS-based control can be optimized by integrating other advanced algorithms, such as genetic algorithms or ant colony algorithms, to reduce fluctuations, phase shifts, and response time. Additionally, the parameters of the MRAS controller's PID regulators can be fine-tuned to achieve better speed regulation and superior signal quality.

In Table 3, a comprehensive overview of the performances of DTC and DTC-MRAS is provided.

Table 3. Performances of DTC and DTC-MRAS.

	Performances	**DTC**	**DTC-MRAS**
Speed (Rad/s)	Response time (s)	0.80	0.6
Torque (Nm)	Ripples (Nm)	2.1	2.9
	Overshoot (Nm)	7	8
	Undershoot (Nm)	14	16
Current (A)	THD (%)	9.76	11.40

DTC (Direct Torque Control) is faster than DTC-MRAS (Model Reference Adaptive System), as shown in Table 3. It is recorded at 0.80 rad/s while DTC-MRAS is noted to be less than 0.6 rad/s. DTC has also been found to respond quicker than DTC-MRAS, taking only 2.1 seconds versus 2.9 seconds, respectively. When comparing torque performance, DTC has a peak of 7 Nm, whereas DTC-MRAS peaked at 8 Nm; however, DTC had a lower dip in torque with an undershoot of 14 Nm compared to DTC-MRAS's undershoot of 16 Nm. Therefore, it can be concluded that DTC outperforms DTC-MRAS in both response time and torque performance. It is observed that the THD of DTC-MRAS control (11.40%) is higher than that of DTC control (9.76%). This difference can be explained by the presence of noise and ripples affecting torque, stator currents, flux, and speed. A spectral analysis of the currents is essential for calculating THD and ensuring a consistent evaluation.

Due to time-related effects associated with sampling, the real-time operation of the 1104 space card requires a sampling frequency between 1 kHz and 10 kHz to drive the inverter and start the machine. It is observed that as the sampling frequencies decrease (from 100 kHz to 10 kHz), the noise in the estimated speed signal increases.

This also leads to increased ripples in all machine parameters, even in sensorless operation. This issue can be mitigated by using PI control based on a genetic algorithm or a swarm intelligence algorithm, even when employing the ANN algorithm. The figures illustrate the fluctuations in the machine's main characteristics, such as rotor speed, stator electrical current, magnetic flux, and mechanical torque. This section describes the results of the DTC control using the MRAS algorithm and the optimized DTC, along with a comparison of the two approaches. The results show that the machine can start under variable loads (-10 Nm to 10 Nm) using one or more control methods and that the speed precisely matches the reference variable, oscillating between -157 rad/s and 157 rad/s. The machine performs better, especially with the classic DTC control, which results in lower mechanical torque and a more sinusoidal current with reduced ripple.

6 Practical Validation and Interpretation

A basic, realistic approach can be constructed that may provide a platform for sequential testing of the required changes and assessing the feasibility of the nonlinear control techniques DTC and DTC-MRAS. The control board uses the DS1104 "R&D" dSPACE control board. The computer has installed a Real-Time Interface RTI library to communicate between the dSPACE board and a physical system in the worked example simulation. This element sends signals from the simulation world to the physical system. TTL (PWM) logical signals between 0 and 5 V were produced by the board's physical system and controlled the application and signal processing. The TTL-CMOS control boards must be properly insulated, powered at 0/15 V, to drive the IGBTs in an inverter together with the slave DSP TMS320F240. With some specialized blocks from the RTI Toolbox library, the designer can develop a real-time application based on emulation software packages (MATLAB). Here we show a diagram of the DS1104 and asynchronous machine connection, as well as images of the experimental configuration. The control board and RTW tool were utilized together to perform experimental investigations.

Using resistive loads of -10 Nm, -5 Nm, 0 Nm, 5 Nm, and 10 Nm, the system's performance at the dSPACE DS1104 facility can be verified from its previous objectives by evaluating the machine's performance under multiple operating conditions. After running a speed variator up and down to the DTC and DTC-MRAS, as well as to the proposed asynchronous machine, both with and without loads, it can be seen in Figures 14 to 19 that the results in a controlled environment were good. It can be seen that when the speed was altered in each direction quickly from 0 to 157 rad/s and back from -157 rad/s and back to 0, it did so quickly and did not exceed the limits. Unlike standard DTC control, the neural network approach will eliminate speed profile spikes that arise due to transient changes in reference values when a variable torque is applied. In addition, it is worth recognizing that the sinusoidal shape of the stator and rotor currents changes along with the load. The simulated results and results obtained from the field in many different board applications are in good conformity, as these figures show.

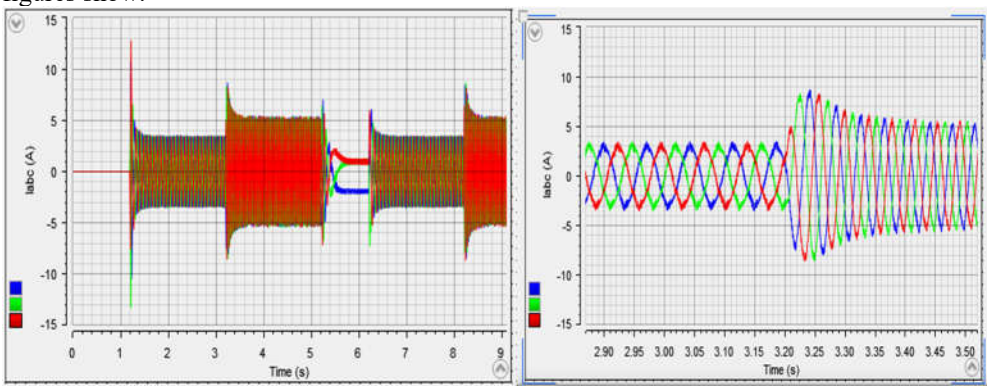

Fig. 14. Waveforms of the stator currents for the DTC control, along with a zoom of the currents.

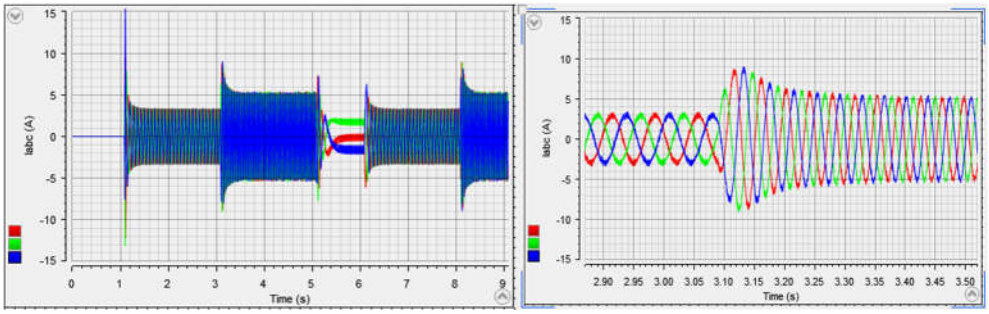

Fig. 15. Waveforms of the stator currents for the DTC-MRAS control, along with a zoom of the currents.

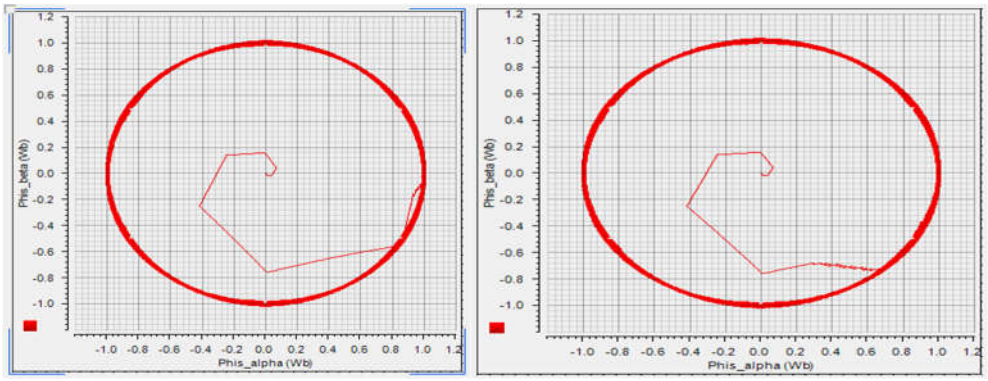

(a) (b)

Fig. 16. Waveforms of the stator flux for the DTC control (a) and the DTC-MRAS control (b).

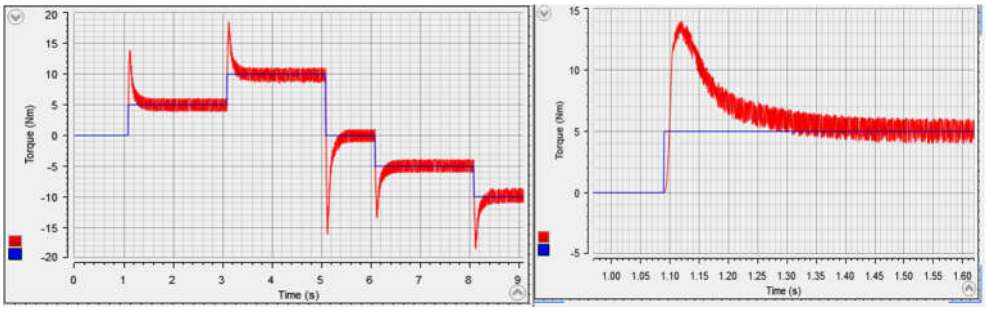

Fig. 17. Torque curves of the DTC controller, along with a zoom.

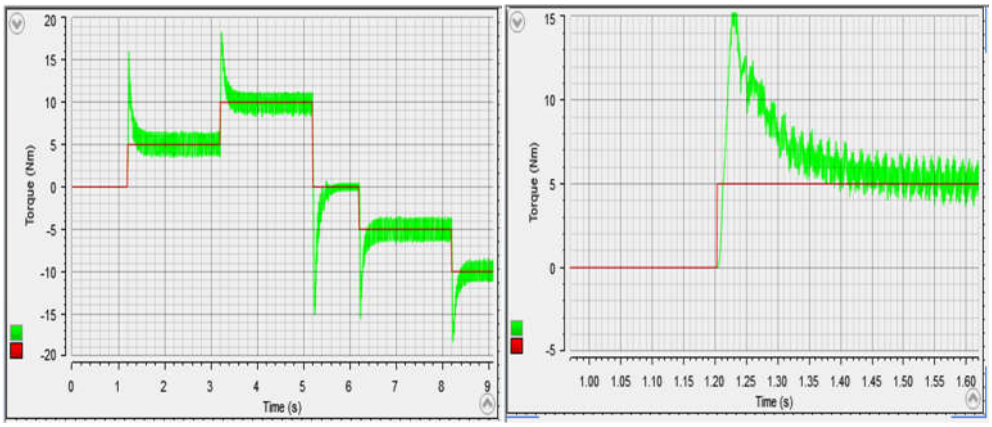

Fig. 18. Torque curves of the DTC-MRAS controller, along with a zoom.

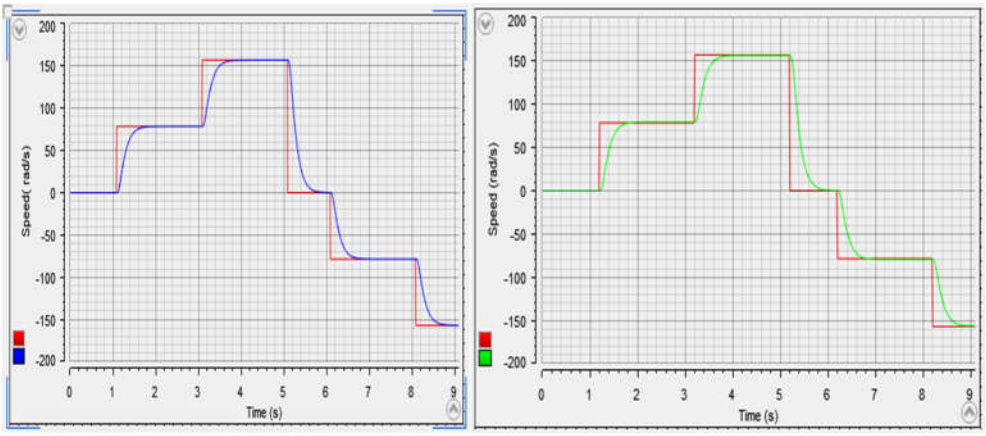

(a) (b)

Fig. 19. Responses to speed variations for the DTC (a) and DTC-MRAS (b).

The figures illustrate the fluctuations in the machine's main characteristics, such as rotor speed, stator electrical current, magnetic flux, and mechanical torque. This section describes the outcomes of the DTC control using the MRAS algorithm, along with a comparison of the two approaches.

The results show that the machine can start under variable loads (-10 Nm to 10 Nm) using one or more control methods and that the speed precisely matches the reference variable between -157 rad/s and 157 rad/s.

The machine performs better, especially with the classic DTC control, which results in lower mechanical torque and a more sinusoidal current with reduced ripple.

7 Conclusions

According to the results, the simulations conducted in the MATLAB/Simulink environment were found to be compatible and reliable. The findings indicate that both the DTC and DTC-MRAS control methods deliver notable performance improvements, particularly in terms of signal quality, torque ripple, response time, and overshoot.
The objective is to implement optimized DTC in conjunction with the MRAS algorithm, eliminating the need for sensors. This approach can be further enhanced through the application of genetic algorithms and particle swarm optimization techniques, which aim to improve the performance of the MRAS estimator.
By doing so, the effectiveness of this control method can be brought in line with traditional DTC approaches. The primary goal of this research has been to control the machine without sensors, thereby optimizing the system. This strategy not only reduces installation costs and minimizes maintenance but also enhances overall performance. Furthermore, this sensorless approach will facilitate testing the machine in real-world environments, which is a key objective for future work.

Appendix

Table 4. The asynchronous machines are parameters.

Symbols	**Values (Unit)**
P_n	1.5Kw
V_s	230v
p	2
f	50Hz
R_s, R_r	1.75Ω,168Ω
L_s	0.424H
L_r	0.424H
L_m	0.404H
f	0.0071kg · m2/s
J	0.018kg.m2

Table 5. Nomenclature.

Parameters	**Description**
$V_{s\alpha}$, $V_{s\beta}$, $V_{r\alpha}$, and $V_{r\beta}$	Stator and rotor voltages in the (α, β) plane
U_{dcs} and U_{dcr}	Stator and rotor direct voltages
$I_{s\alpha}$, $I_{s\beta}$, $I_{r\alpha}$, and $I_{r\beta}$	Stator and rotor currents in the (α, β) plane
$\Psi_{s\alpha}$, $\Psi_{s\beta}$, $\Psi_{r\alpha}$, and $\Psi_{r\beta}$	Stator and rotor flux in (α, β) plane
R_s, R_r	Stator and rotor resistors
L_s, L_r	Stator and rotor inductors
L_m	Mutual Inductance
P	Number of pairs of poles
ω_r	Rotor angular speed
ω_s	Stator angular speed
Ω	Rotation speed
T_{em}	Electromagnetic torque
T_r	Resistant torque
F	Viscous friction coefficient

References

1. Reza CMFS, Islam MD, Mekhilef S (2014) A review of reliable and energy efficient direct torque controlled induction motor drives. Renew Sustain Energy Rev 37:919 932.

2. Jannati M, Anbaran SA, Asgari SH, Goh WY, Monadi A, Aziz MJA, Idris NRN (2017) A review on variable speed control techniques for efficient control of single-phase induction motors: evolution, classification, comparison. Renew Sustain Energy Rev 75:1306 1319.

3. Krishna SM, Daya JL, Padmanaban FS, Mihet-Popa L (2017) Real-time analysis of a modified state observer for sensorless induction motor drive used in electric vehicle applications. Energies 10(8):1077.

4. Das, S., Kumar, R., & Pal, A. (2018). MRAS-based speed estimation of induction motor drive utilizing machines and q-circuit impedances. IEEE Transactions on Industrial Electronics, 66(6), 4286-4295.

5. Blaschke F (1972). The principle of field orientation is applied to the new Transvector closed-loop control system for rotating field machines. Siemens Rev 34(5):217–220.

6. Takahashi I, Noguchi T (1986) A new quick-response and high-efficiency control strategy of an induction motor. IEEE Trans Ind Appl 5:820-827.

7. Hasse K (1968) Zum dynamischen Verhalten der Asynchronmaschine bei Betrieb mit variabler Standerfrequenz und Standerspannung. ETZ-A 89:77.

8. Korzonek, M., Tarchala, G., & Orlowska-Kowalska, T. (2019). A review of MRAS-type speed estimators for reliable and efficient induction motor drives. ISA transactions, 93, 1-13.

9. Dos Santos TH, Da Silva IN, Goedtel A, Castoldi MF (2019). Neural speed estimation applied to stator flux-oriented control drives. Electric Power Compon Syst 47(9–10):798–809.

10. Yi B, Kang L, Jiang K, Lin Y (2013). A two-stage Kalman filter for sensorless direct torque-controlled PM synchronous motor drive. Math Probl Eng. https://doi.org/10.1155/2013/768736.

11. Gunabalan R, Subbiah V, Reddy BR (2009) Sensorless control of induction motor with extended Kalman filter on TMS320F2812 processor. Int J Recent Trends Eng 2(5):14.

12. Shinohara A, Inoue Y, Morimoto S, Sanada M (2016). Direct calculation method of reference flux linkage for maximum torque per ampere control in DTC-based IPMSM drives. IEEE Trans Power Electron 32(3):2114–2122.

13. Karlovský P, Lettl J (2017). Improvement of DTC performance using the Luenberger observer for flux estimation. In: 2017 18th international scientific conference on electric power engineering (EPE). IEEE, pp 1–5.

14. El Merrassi, W., Abounada, A., & Ramzi, M. (2021). Advanced speed sensorless control strategy for induction machine based on the neuro-MRAS observer. Materials Today: Proceedings, 45, 7615-7621.

15. El Mahfoud M, Bossoufi B, El Ouanjli N, Mahfoud S, Taoussi M (2021) Three-speed controllers of direct torque control for a doubly fed induction motor drive–A comparison. Electrica 21(1):129–142.

16. Gundewar, S.K., Kane, P.V.: Condition monitoring and fault diagnosis of induction motor. J. Vibr. Eng. Technol. 9(4), 643–674 (2020). https://doi.org/10.1007/s42417-020-00253-y 2.

17. Konar, P., Chattopadhyay, P.: Multi-class fault diagnosis of induction motor using Hilbert and wavelet transform. Appl. Soft Comput. 30, 341–352 (2015). https://doi.org/10.1016/j.asoc. 2014.11.06.

18. Puche-Panadero, R., Martinez-Roman, J., Sapena-Bano, A., Burriel-Valencia, J., Riera-Guasp, M.: Fault diagnosis in the slip–frequency plane of induction machines working in time-varying conditions. Sensors (Switzerland) 20(12), 1–25 (2020). https://doi.org/10.3390/ s20123398.

19. El Ouanjli, N., Mahfoud, S., Bhaskar, M. S., El Daoudi, S., Derouich, A., & El Mahfoud, M. (2022). A new intelligent adaptation mechanism of MRAS based on a genetic algorithm applied to speed sensorless direct torque control for an induction motor. International Journal of Dynamics and Control, 10(6), 2095-2110.

20. Boyar, A., Kabalci, E., & Kabalci, Y. (2024). Sensorless speed controller of an induction motor with MRAS-based model predictive control. Computers and Electrical Engineering, 118, 109350.

21. Ammar A, Bourek A, Benakcha A (2017) Nonlinear SVM-DTC for induction motor drive using input-output feedback linearization and high order sliding mode control. ISA Trans 67:428–442.

22. Wu S, Liu Z, Su H (2017). Adaptive sliding mode sensorless vector control of an induction motor using a sliding mode MRAS observer. In: 2017 36th Chinese Control Conference (CCC). IEEE, pp 9124–9129.